Journal of Ceramic Processing Research. Vol. 10, No. 6, pp. 832~839 (2009)

J O U R N A L O F
Ceramic Processing Research

An easy one-pot synthesis of structurally controlled aluminum hydroxide particles from an aqueous sodium aluminate solution

Tae Sun Chang, Jeong Hyeon Na, Chan Yoon Jung and Sang Man Koo*
Department of Chemical Engineering, Hanyang University, Seoul, Korea

Here, we describe an easy one-step process for producing structurally controlled aluminium hydroxide nano-materials with various morphologies and porosities from an aqueous sodium aluminate ($NaAlO_2$) solution. Crystalline urchin-shaped hollow particles with a boehmite structure were prepared using a simple precipitation process at 60 °C. By lowering the reaction temperature, the formation process for urchin-shaped hollow particles could be monitored: 1) the generation of thin-film shaped materials, 2) the transformation into nano-rods, and 3) the formation of hollow particles. With heat treatment at 700 °C, the urchin-shaped hollow particles were completely converted to γ-Al_2O_3 particles without changing their morphology. Rod-shaped products with a dawsonite structure could be obtained by the slow evaporation of boehmite nanorods in an aqueous alcoholic solution. The sodium dawsonites were converted to the diaoyudaoite phase with heat treatment at 900 °C, exhibiting a disruption in their morphology. In addition, non-crystalline porous spherical particles were also prepared using simple precipitation at 12 °C. Heat treatment at 900 °C transformed the amorphous spherical particles into γ-Al_2O_3 particles, maintaining their spherical morphologies.

Key words: sodium aluminate, urchin-shaped hollow particle, porous particles.

Introduction

Aluminum oxides have been investigated extensively for scientific and industrial applications such as for catalysts, sorbents, as ceramics, and for supporting materials. [1-6] Among the various types of alumina, nanostructured aluminas are interesting because of their useful characteristics such as high elastic moduli, thermal and chemical stability, and optical properties. [7-11] The conventional preparation method for Al_2O_3 is the dehydration of aluminum hydroxides, especially AlOOH (boehmite), where the morphology and size of the final Al_2O_3 strongly depend on the green precursor used during the conversion process. [12, 13] Various synthetic methods for the preparation of aluminum hydroxides have been developed, including vapor phase and liquid phase syntheses, and several types of boehmite such as particles, fibers, rods, tubes, and belts have been synthesized. [14-16] Template-based synthesis, an emulsion process, a hydrothermal method, chemical vapor deposition, and an electrochemical process were employed for the preparation of one-dimensional (1D) nanostructures. [14, 16-19] Recently, alumina nanomaterials with highly ordered structures have been prepared by several research groups. Hollow, core-shell, urchin-shaped, and cantaloupe-like AlOOH superstructures were prepared using a hydrothermal method in the presence of structure-directing reagents such as amphiphilic block copolymers and trisodium citrate dehydrates. [20-22] However, these surfactant-based hydrothermal methods either involved multi-step synthesis and harsh reaction conditions, or produced a product with heterogeneous impurities which limit their industrial application. Therefore, it remains a major challenge to develop a simple, template-free one-step solution route for the preparation of three-dimensionally ordered structures.

In this study, we report a simple synthetic route for the production of crystalline aluminum hydroxide nanorods, urchin-shaped hollow particles, and porous spherical particles. By simply controlling the reaction conditions such as concentration, temperature, dropping rate, and evaporation rate, aluminum hydroxide nanomaterials with different morphologies and porosities were obtained from an aqueous sodium aluminate ($NaAlO_2$) solution. Non-crystalline spherical particles were prepared at a low temperature of 12 °C, while crystalline urchin-shaped hollow particles with a boehmite structure were obtained at 60 °C. The urchin-shaped hollow particles were completely converted to γ-Al_2O_3 particles without a morphological change after heat treatment at 700 °C. Rod-shaped products were obtained by the slow evaporation of boehmite nanorods in an aqueous alcoholic solution.

Experimental Procedure

Urchin-shaped hollow particles

0.1 g of sodium aluminate (Sukgyung, 92%, $NaAlO_2$, 1.12 mmole) was dissolved in 38 ml of deionized water while stirring. While maintaining the solution at 60 °C, 400 ml of ethyl alcohol (Sanchun Chemical, 95 wt%)

*Corresponding author:
Tel : +82-2-2220-0527
Fax: +82-2-2281-4800
E-mail: sangman@hanyang.ac.kr

was added at a dropping rate of 1.33 mls^{-1}. Upon the complete addition of the ethyl alcohol, the solution became turbid and the suspension was stirred for 1 hour. The reaction mixture was filtered, washed with deionized water several times, and dried at 120 °C in a vacuum oven for 24 hours. The yield after drying was 71.2%.

Porous spherical particles

0.1 g of sodium aluminate (Sukgyung, 92%, $NaAlO_2$, 1.12 mmole) was dissolved in 38 ml of deionized water while stirring. While maintaining the solution at 12 °C, 400 ml of ethyl alcohol (Sanchun Chemical, 95 wt%) was added at a dropping rate of 1.33 mls^{-1}. Upon the complete addition of the ethyl alcohol, the solution became turbid and the suspension was stirred for 1 hour. The reaction mixture was filtered, washed with deionized water several times, and dried at 120 °C in a vacuum oven for 24 hours. The yield after drying was 52.6%.

Rod-shaped products

0.1 g of sodium aluminate ($NaAlO_2$, 1.12 mmole) was dissolved in 38 ml of deionized water while stirring. While maintaining the solution at 20 °C, 400 ml of ethyl alcohol (95 wt%) was added at a dropping rate of 8.0 mls^{-1}. After the complete addition of the ethyl alcohol, the solution was evaporated in air for 24 hours. The optimum evaporation rate of the alcohol was 0.54 mlh^{-1}. The reaction mixture was filtered, washed with deionized water several times, and dried at 120 °C in a vacuum oven for 24 hours. The yield after drying was 49.4%.

Characterization

The crystallinity and structural changes of the products were confirmed by X-ray diffractometry (XRD, Rigaku, Rint-200) using CuKa radiation at 40 kV and 100 mA. The sizes and morphologies of the reaction intermediates and products were examined with a field emission scanning electron microscope (FE-SEM, JEOL JSM-6700F) and a transmission electron microscope (TEM, JEOL JEM-3010 and JEM-1010). The chemical analyses were conducted using a nuclear magnetic resonance spectrometer (NMR, Bruker, 400 MHz) and Fourier transform infrared spectrometer (FT-IR, AAB, FTLA2000). Thermal analyses of the products were performed with a thermo-gravimetric analyzer (TGA, Bruker, TG-DTA2000SA). The nitrogen absorption and desorption isotherms at 77 K were measured using a Micromeritics ASAP-2010 analyzer.

Results and Discussion

Urchin-shaped hollow particles

Urchin-shaped hollow particles consisting of boehmite nanorods were prepared by the slow addition of ethyl alcohol into an aqueous sodium aluminate solution. Initially, the transparent solution became turbid during the addition of the alcohol, and a white suspension was obtained after the alcohol addition was complete. After 2 hours of stirring at room temperature, thin film-shaped materials were formed which could be identified using electron microscopy. After 12 hours of reaction, these thin film-shaped materials converted to nanorods. After 20 hours of reaction, the nanorods self-assembled into urchin-shaped hollow particles. SEM and TEM images of the products at each reaction time are shown in Fig. 1. XRD analyses indicated that these intermediate nanofilms and nanorods had a boehmite (AlOOH) structure (JCPDS No. 17-0940). Several research

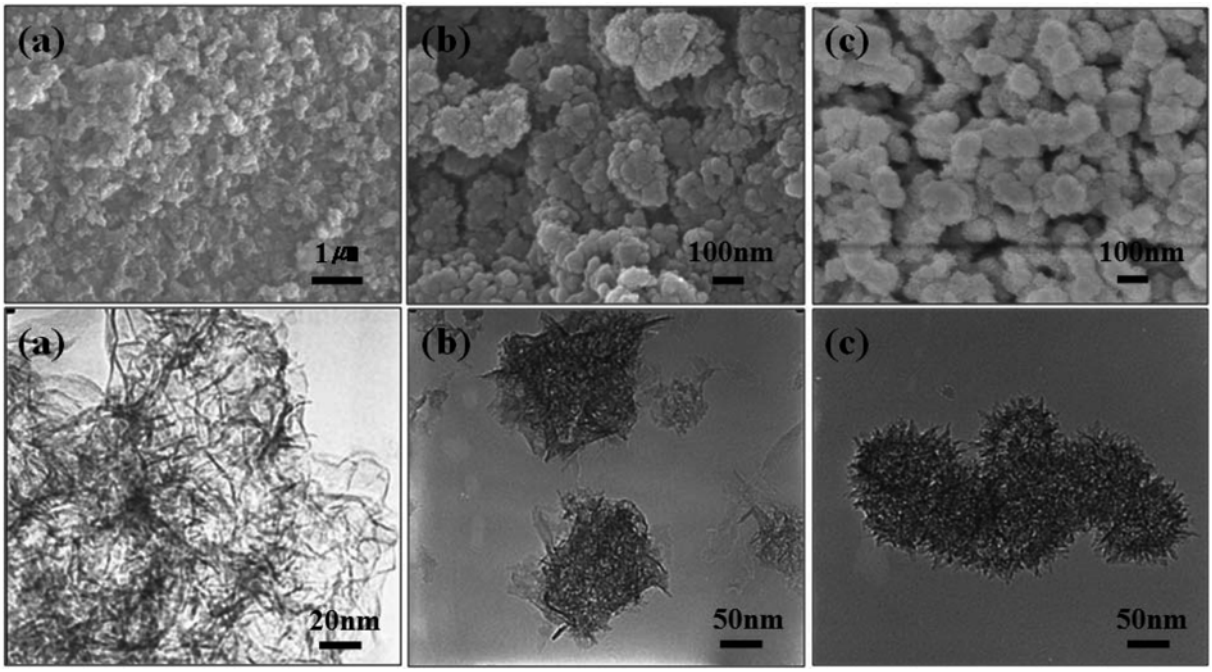

Fig. 1. SEM and TEM images of urchin-shaped particles prepared at room temperature after (a) 2 h, (b) 12 h, and (c) 20 h.

groups previously reported that the transformation of the nanotubes resulted from the sticking of lamellae followed by scrolling, dissolution, and growth from the meta-stable lamellae structure. [23] The formation mechanism of the nanorods in this study confirmed a similar transformation process. When the reaction temperature was raised to 60 °C, the reaction proceeded so quickly that urchin-shaped hollow spherical particles were formed in less than 1 hour. An additional increase in reaction temperature to 75 °C did not change the morphology of the particles, but the thickness of the nanorods increased (see Fig. 2). The XRD spectrum of the urchin-shaped hollow particles obtained at high reaction temperatures exhibited the diffraction patterns of AlOOH, in which the shapes of the peaks grew more narrower and more intense as the reaction temperature was increased. Extending the reaction time also caused a similar effect, which yielded urchin-shaped particles consisting of thicker nanorods as shown in Fig. 3. The effect of the alcohol dropping rate on the formation of the particles was investigated. When the dropping rate was increased (from 1.47 mls^{-1} to 10.5 mls^{-1}), smaller particles with sizes less than 100 nm were formed. However, undeveloped urchin-shaped hollow particles with un-assembled nanorods were observed. The increase in dropping rate made the nanorods precipitate more quickly, preventing the secondary formation of urchin-shaped hollow particles. When a slower dropping rate of 0.57 mls^{-1} was employed, thicker urchin-shaped hollow particles with sizes larger than 100 nm were obtained (see SI). The effect of the precipitating solvent on the morphology of the product was also investigated. When methyl alcohol was used instead of ethyl alcohol, irregularly shaped thin flake-like products were obtained, and XRD analysis revealed that the product was aluminum hydroxide methoxide ($AlO(OH)_{0.5}(OCH_3)_{0.5}$, JCPDS No. 22-1538). When isopropyl alcohol was used, plate-shaped aluminum hydroxide ($Al(OH)_3$) was formed (see SI).

The IR spectrum of the urchin-shaped hollow particles exhibited vibrational absorption bands at 3360, 3110,

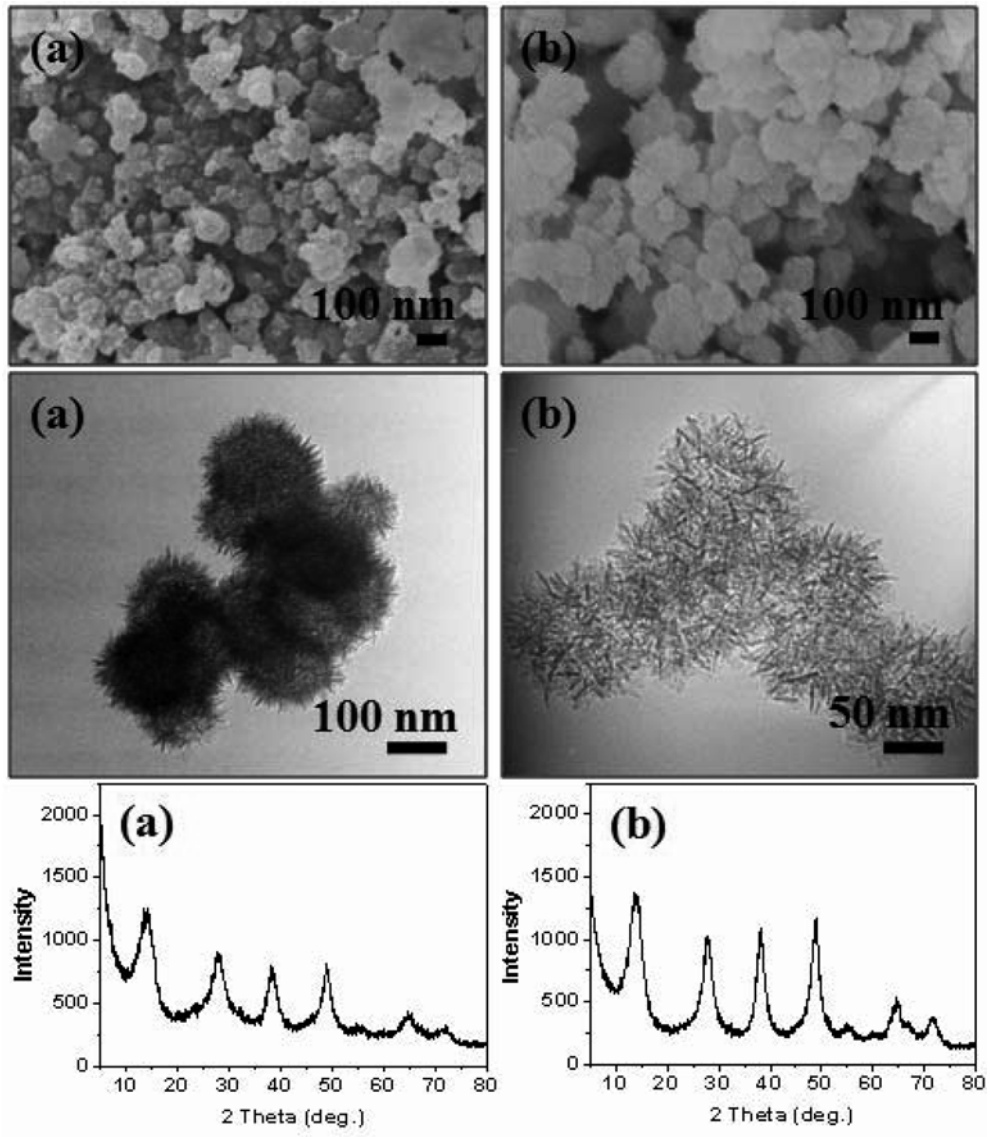

Fig. 2. SEM images, TEM images, and XRD patterns of urchin-shaped hollow particles prepared at (a) 60 °C and (b) 75 °C.

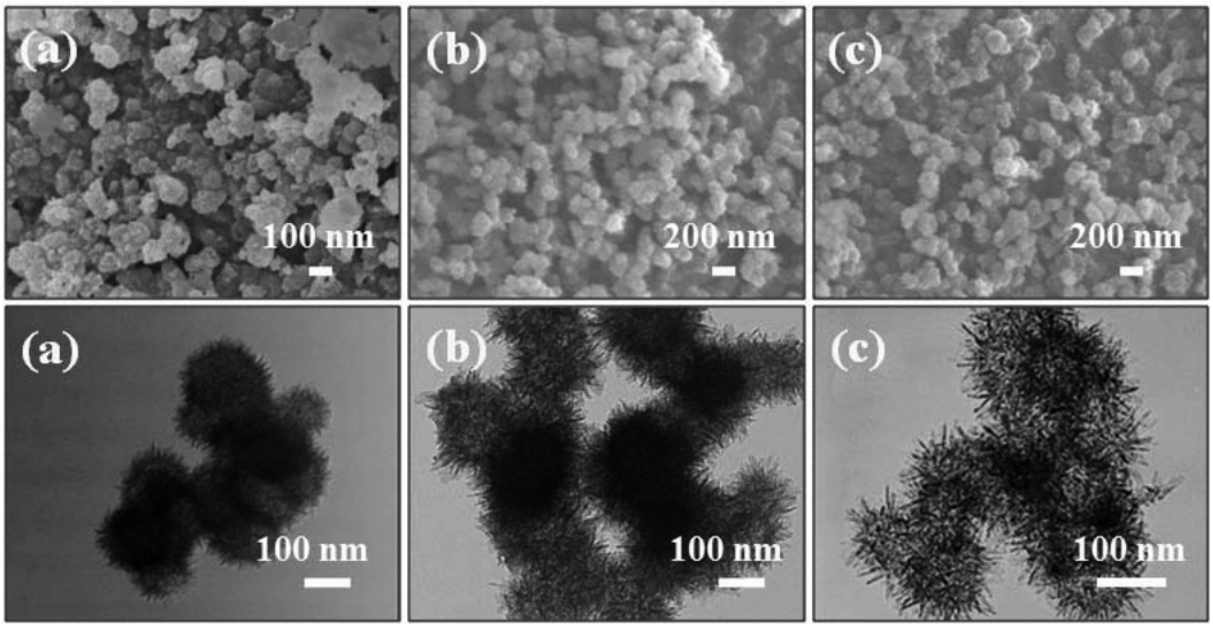

Fig. 3. SEM and TEM images of urchin-shaped particles prepared at 60 °C after (a) 1 h, (b) 24 h, and (c) 72 h.

2090, 1640, 1160, 1080, 739, and 625 cm^{-1}, which matched precisely with previously reported values of boehmite, γ-AlOOH. [24] The intense bands at 3360 and 3099 cm^{-1} were assigned to the asymmetric and symmetric O-H stretching vibrations from (O)Al-OH. The band at 1080 cm^{-1} and the shoulder at 1160 cm^{-1} were ascribed to symmetric and asymmetric Al-O-H bending. The broad band around 2090 cm^{-1} was known to come from the combination band. The small band at 1640 cm^{-1} was assigned to the bending mode of the adsorbed water molecules. Weak absorption bands at 1510 and 1400 cm^{-1} from adsorbed carbonates were observed. The shoulder at 750 cm^{-1} and the band at 630 cm^{-1} from the vibration modes of Al-O indicated an octahedral AlO_6 structure. The octahedral structure of the AlOOH in the urchin-shaped particles was also confirmed by NMR analysis. The CP-MAS [27] Al NMR of the particles showed only one absorption peak at 7.5 ppm from the octahedral AlO_6 unit [25, 26] (see SI).

The TGA curve of the urchin-shaped hollow particles showed two weight losses. The first one at 200-400 °C was due to adsorbed water molecules, and the second one at 400-500 °C was attributed to the phase transformation of boehmite (AlOOH) to Al_2O_3, as found in the literature. [27] The theoretical percent of weight loss for the conversion of AlOOH to Al_2O_3 is 15%. The experimental value of 23% may reflect the additional losses of the adsorbed water and carbonates. Electron microscopy images and XRD patterns of the particles after heat treatment at 900 °C showed that the boehmite AlOOH particles were transformed to γ-Al_2O_3, maintaining their urchin-shaped structures. (see Fig 4) It has been reported that the phase transformation of AlOOH to γ-Al_2O_3 occurs at temperatures between 400 and 700 °C. [27, 28] The calcination of these particles at 1100 °C produced a mixture of the α- and γ-Al_2O_3 phases. The morphology of the urchin-shaped particles was destroyed, and melting between the particles occurred at this temperature.

Brunauer-Emmett-Teller (BET) gas-sorption measurements were conducted to examine the internal structures of the urchin-shaped hollow particles before and after heat treatment as shown in Fig. 5. N_2 adsorption and desorption isotherms of both products exhibited similar Type IV hysteresis at relative pressures of P/P_0 above 0.5 and 0.45, respectively. This type of hysteresis loop is known to be associated with hollow particles that have mesoporous shells. Barret-Joyner-Halenda calculations for the pore size distribution, derived from the desorption data, revealed that the average pore diameters were 8.1 and 7.8 nm for the as-prepared and calcined particles, respectively. The BET surface areas of the samples calculated from N_2 isotherms at 77 K were found to be 192 and 266 m^2g^{-1} for the as-prepared and calcined materials, respectively. This indicates that the heat treatment did not change the morphologies of the nanorods, while desorption of water molecules and carbonates increased the surface area slightly.

Rod-shaped products

When the suspension obtained after the addition of ethyl alcohol at room temperature was evaporated slowly in air, rod-shaped products were observed. An SEM image, a TEM image, and an XRD pattern of the product are shown in Fig. 6. An SEM and TEM images show that rod-shaped products with an average diameter of 50 nm and lengths of up to 1 μm were formed, although a small amount of irregularly shaped products consisting of nanorods was also observed. The XRD pattern of the rod-shaped products indicate that the major product was a sodium dawsonite ($NaAl(OH)_2CO_3$ JCPDS No.12-0449) with minor AlOOH and $Al(OH)_3$ phases. Dawsonite-type compounds were previously prepared by Zhang *et al*. [29] Hydrothermal

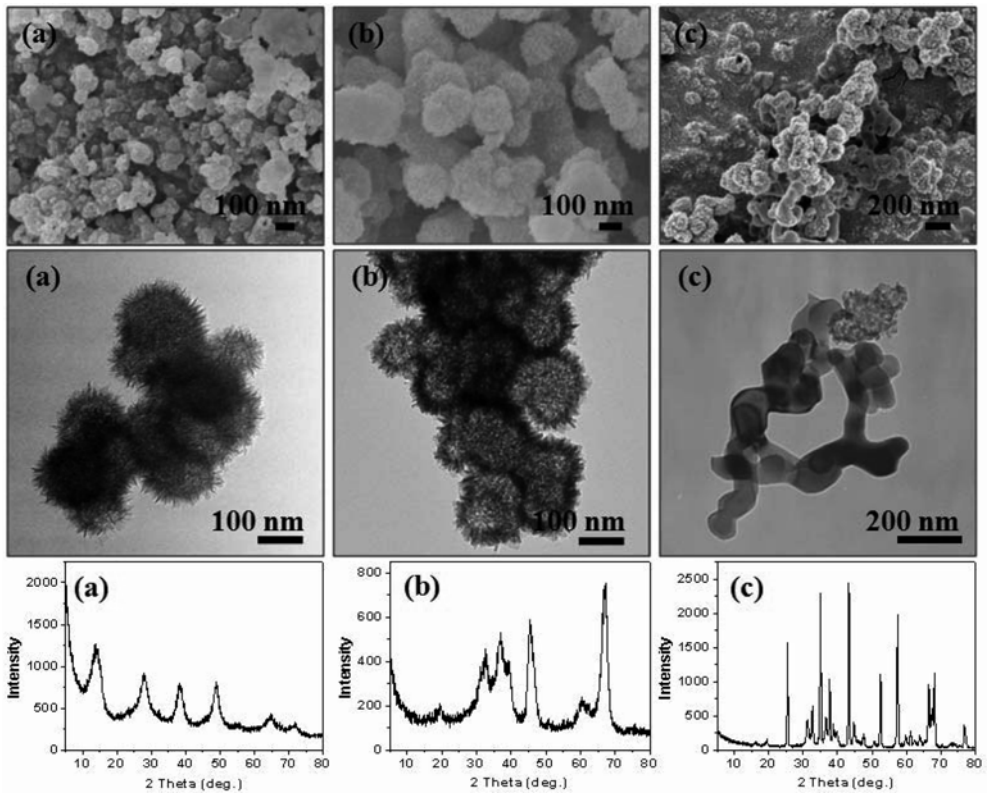

Fig. 4. SEM, TEM images, and XRD patterns of urchin-shaped particles (a) before heat treatment, and after heat treatment at (b) 900 °C, and (c) 1100 °C.

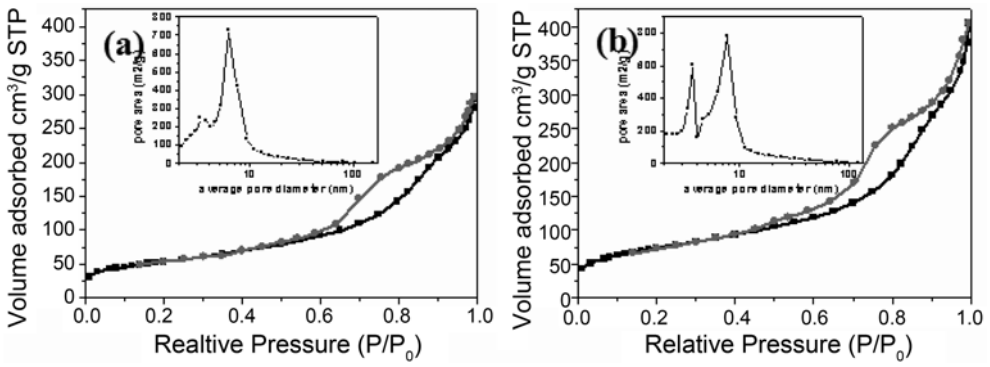

Fig. 5. N_2 adsorption and desorption isotherms of urchin-shaped particles (a) before heat treatment. and (b) after heat treatment at 900 °C for 1 hour in air.

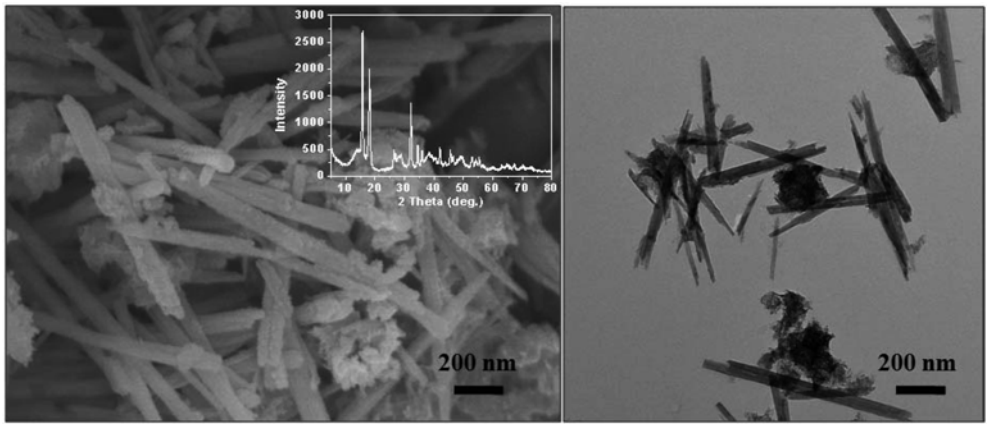

Fig. 6. SEM, TEM images and XRD pattern of the rod-shaped particles.

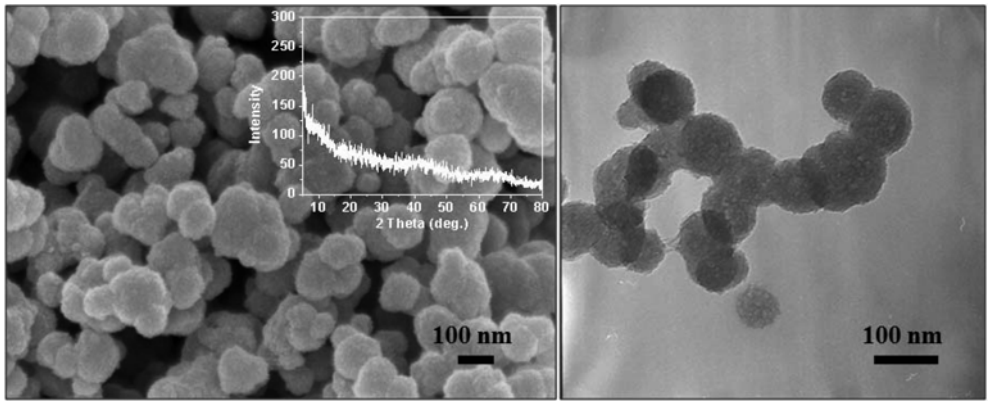

Fig. 7. SEM, TEM images and XRD pattern of amorphous spherical particles.

syntheses were employed to produce rod-shaped dawsonites from $Al(OH)_3$ and $MHCO_3$ (M = Na, K, NH_4). Zhang *et al.* also reported the optimum conditions for the formation of rod-shaped dawsonites, and investigated the structures and morphologies using XRD and TEM. In our study, rod-shaped dawsonite compounds were obtained through the slow evaporation of AlOOH nanorods. Their formation is explained as follows: 1) in the first step, gaseous CO_2 in air was dissolved into a basic AlOOH solution, then 2) dissolved CO_2 was converted to $NaHCO_3$ with NaOH in solution, 3) $NaHCO_3$ reacted with AlOOH to produce $NaAl(OH)_2CO_3$, and finally, 4) the growth of rod-shaped dawsonites occurred through a solvent evaporation.

The chemical structure and thermal behavior of the rod-shaped dawsonites were investigated. CP-MAS [27] Al NMR spectra of the dawsonites exhibited three absorption peaks at 7.5, –7.4, and –21 ppm. The main peak at 7.5 ppm corresponded to the octahedral Al structure, as described earlier, and the two shoulders at –7.4 and –21 ppm come from the Al-CO_3 structures. The IR spectra of the rod-shaped dawsonites showed vibrational absorption bands at 3290, 3100, 2090, 1580, 1400, 1220, 1160, 1100, 1070, 955, 847, 692, 625, and 548 cm^{-1}. The strong band at 3290 cm^{-1} was assigned to the asymmetric H-O(Al) stretching vibration, and the narrow peak width with a strong intensity indicated well-ordered O-H structures. Absorption peaks at 1070, 625, and 548 cm^{-1} were from Al-OH and AlO_6 bending vibrations, respectively. Other intense bands at 1580, 1400, 1100, 955, 847, and 692 cm^{-1} were attributed to (Al)-CO_3 units (see SI).

The TGA curve of the rod-shaped dawsonites showed two periods of weight loss. The first loss at 330 °C was attributed to the removal of CO_2 and H_2O during the conversion of $NaAl(OH)_2CO_3$ to $NaAl_{11}O_{17}$. The second weight loss above 600 °C was due to the volatilization of Na_2O, which was also a decomposition by-product. The theoretical percent of weight loss for this conversion is 37%. The experimental value of 58% might indicate that the conversion was incomplete, yielding the Al_2O_3 phase as a by-product. SEM and TEM images of the calcined products at 900 °C exhibited micrometer-sized plate-shaped material along with a small amount of the rod-shaped product. XRD spectra of this product indicated that the diaoyudaoite phase ($NaAl_{11}O_{17}$, JSPDS No. 32-1033) was formed (see SI). N_2 adsorption and desorption isotherms of the rod-shaped products before and after heat treatment exhibited type III hysteresis, which indicates that the product was a dense material, as expected from its morphology and crystallinity (see SI).

Amorphous spherical particles

When the reaction was carried out at 12 °C, porous spherical particles were formed after 1 hour of stirring. An SEM image, a TEM image, and an XRD pattern of the product are shown in Fig. 7. The TEM image shows that porous particles with an average size of 80 nm were formed, although polydispersed particles from the agglomeration of the primary spherical particles were also observed in the SEM image. XRD analysis indicated that the spherical particles were amorphous. IR spectra of the particles exhibited similar vibrational absorption patterns to those seen in the urchin-shaped particles, although the peak at 1600 cm^{-1} from H_2O was more intense. CP-MAS [27] Al NMR spectra of the porous particles showed three resonance peaks at 64, 34, and 8 ppm. The strong peak at 8 ppm was from octahedral Al, while the two peaks at 34 and 64 ppm were attributed to penta- and tetra-coordinated Al, respectively, as stated in the literature [25, 26] (see SI).

Changes in the alcohol dropping rate had an effect on the formation and morphology of the resultant particles. When the dropping rate was increased from 1.47 mls^{-1} to 10.5 mls^{-1}, irregularly shaped products were formed along with a small amount of primary particles, while polydispersed spherical particles were obtained when the dropping rate was decreased to 0.57 mls^{-1} (see SI). In addition, an increase in the reactant concentration produced plate-shaped products which were identified as the crystalline $Al(OH)_3$ phase by XRD analysis. Similar plate-shaped products from the $Al(OH)_3$ phase could also be obtained by dropping isopropyl alcohol instead of ethyl alcohol. When methyl alcohol was used, lamellae-shaped products with the AlOOH phase were formed (see SI).

The TGA curve of the porous particles showed two periods of weight loss. The first period of weight loss

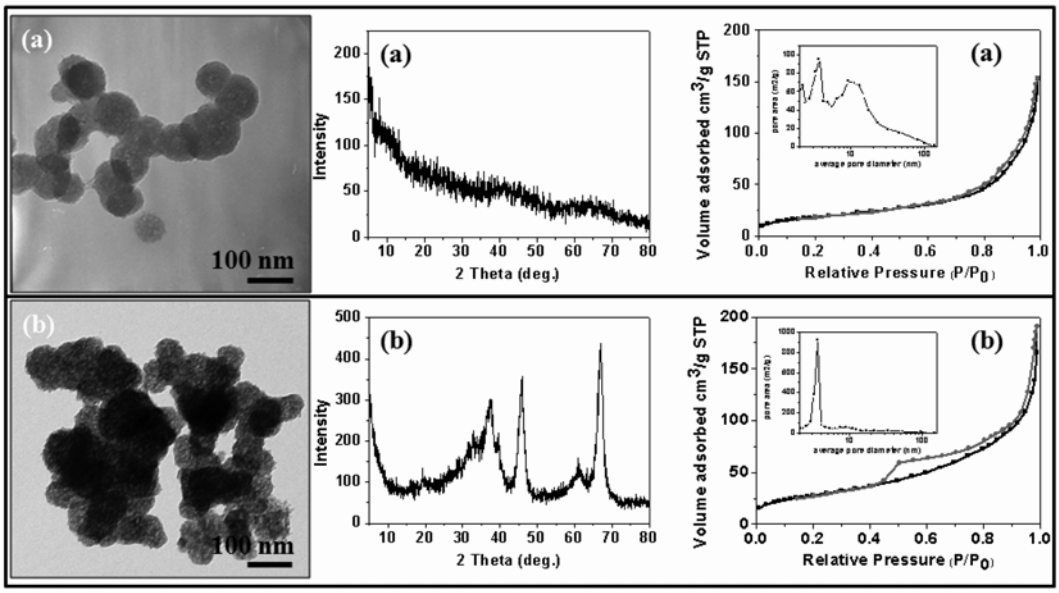

Fig. 8. TEM images, XRD patterns, and N_2 adsorption/desorption isotherms of spherical particles (a) before heat treatment, and after heat treatment at (b) 900 °C for 1 hour under air condition.

at 150-400 °C was caused by the loss of adsorbed H_2O molecules, and the second at 950 °C was attributed to dehydrated H_2O molecules from the transformation to γ-Al_2O_3 (JCPDS No. 29-0063). XRD patterns of the heat treated particles exhibited no discernable phase development until 600 °C, while the XRD pattern of the particles calcined at 800 °C indicated the development of a diffraction pattern corresponding to γ-Al_2O_3. The complete transformation of the porous particles to γ-Al_2O_3 was observed at 900 °C. SEM and TEM images of the calcined product at 900 °C showed that the morphology of the particles was maintained, although the size of the internal pores was somewhat increased (see Fig 8). The N_2 adsorption and desorption isotherms of the porous particles before and after heat treatment exhibited type II and type IV hysteresis loops associated with porous and mesoporous materials, respectively. This result was also consistent with TEM observations of porous particles before and after heat treatment. The BET surface areas and average pore sizes of the samples calculated from N_2 isotherms at 77 K were found to be 64 m^2g^{-1} and 10.3 nm for as-prepared particles, and 96.6 m^2g^{-1} and 7.8 nm for the calcined material.

Conclusions

Aluminum hydroxides with various types of structures, morphologies, and porosities were prepared from an aqueous sodium aluminate ($NaAlO_2$) solution using a simple precipitation process. Crystalline urchin-shaped hollow particles with a boehmite structure were prepared at 60 °C. By lowering the reaction temperature, the formation process for urchin-shaped hollow particles from nanorods could be monitored. By heating at 700 °C, the urchin-shaped hollow particles were completely converted to γ-Al_2O_3 particles without changing their morphology. Rod-shaped products with a dawsonite structure were obtained by the slow evaporation of boehmite nanorods in an aqueous alcoholic solution. The sodium dawsonites were converted to the diaoyudaoite phase with heat treatment at 900 °C, exhibiting a disruption in their morphology. In addition, non-crystalline porous spherical particles were prepared at 12 °C. The increase in sodium aluminate concentration produced irregularly shaped beyerite (γ-$Al(OH)_3$) particles. Heat treatment at 900 °C transformed amorphous spherical particles into γ-Al_2O_3 particles, maintaining their spherical morphologies.

Acknowledgments

This research was supported by a grant from the Fundamental R&D Program for Core Technology of Materials funded by the Ministry of Commerce, Industry and Energy, Republic of Korea

References

1. A.M.A. Cruz and J.G. Eon, Appl. Catal. A-Gen 167 (1990) 203-213.
2. Z. Ecsedi, I. Lazău and C. Păcurariu, Microporous Mesoporous Mat. 118 (2009) 453-457.
3. Y. Kim, C. Kim, I. Choi, S. Rengaraj and J. Yi, Environ. Sci. Technol. 38[3] (2004) 924-931.
4. K.V.P.M. Shafi, A. Ulman, J. Lai, N.L. Yang and M.H. Cui, J. Am. Chem. Soc. 125[14] (2003) 4010-4011.
5. P. Kim, J.B. Joo, H. Kim, W. Kim, Y. Kim, I. K. Song and J. Yi, Catal. Lett. 104 (2005) 181-189.
6. S.M. Kim, Y.J. Lee, J.W. Bae, H.S. Potdar and K.W. Jun, Appl. Catal. A-Gen 348 (2008) 113-120.
7. I.W.M. Brown, M.E. Bowden, T. Kemmitt and K.J.D. MacKenzie, Curr. Appl. Phys. 6 (2006) 557-561.
8. A.C.V. Coelho, H.S. Santos, P.K. Kiyohara, K.N.P. Marcos and P.S. Santos, Mater. Res. 10[2] (2007) 183-189.

9. A. Yamaguchi, K. Hotta and N. Teramae, Anal. Chem. 81 (2009) 105-111.
10. D. Qi, K. Kwong, K. Rademacher, M.O. Wolf and J.F. Young, Nano Lett. 3[9] (2003) 1265-1268.
11. S. Puchegger, F. Dose, D. Loidl, K. Kromp, R. Janssen, D. Brandhuber, N. Hüsing and H. Peterlik, J. Eur. Ceram. Soc. 27 (2007) 35-39.
12. P.K. Sharma, M.H. Jilavi, D. Burgard, R. Nass and H. Schmidt, J. Am. Ceram. Soc. 81[10] (1998) 2732-2734.
13. S.C. Kuiry, E. Megen, S.D. Patil, S.A. Deshpande and S. Seal, J. Phys. Chem. B 109[9] (2005) 3868-3872.
14. J. Zhang, S. Liu, J. Lin, H. Song, J. Luo, E.M. Elssfah, E. Ammar, Y. Huang, X. Ding, J. Gao, S. Qi and C. Tang, J. Phys. Chem. B 110[29] (2006) 14249-14252.
15. E.J. Opila and D.L. Myers, J. Am. Ceram. Soc. 87[9] (2004) 1701-1705.
16. C.Y. To, L.Y. Cheung, Y.F. Li, K.C. Chung, D.H.C. Ong and D.H.L. Ng, J. Eur. Ceram. Soc. 27 (2007) 2629-2634.
17. C.P. Lin, S.B. Wen and T.T. Lee, J. Am. Ceram. Soc. 85[1] (2002) 129-133.
18. D. Deng, R. Tang, X. Liao and B. Shi, Langmuir 24 (2008) 368-370.
19. N. Imanaka, T. Masui and Y. W. Kim, Cryst. Growth Des. 4[4] (2004) 663-665.
20. Y. Feng, W. Lu, L. Zhang, X. Bao, B. Yue, Y. lv and X. Shang, Cryst. Growth Des. 8[4] (2008) 1426-1429.
21. L. Zhang, W. Lu, L. Yan, Y. Feng, X. Bao, J. Ni, X. Shang and Y. Lv, Microporous Mesoporous Mat. 119 (2009) 208-216.
22. X. Wu, D. Wang, Z. Hu and G. Gu, Mater. Chem. Phys. 109 (2008) 560-564.
23. H. Hou, Y. Xie, Q. Yang, Q. Guo and C. Tan, Nanotechnology 16 (2005) 741-745.
24. S. Musiæ, Đ. Dragčević and S. Popoviæ, Mater, Lett. 40 (1999) 269-274.
25. J.H. Kwak, J. Hu, A. Lukaski, D.H. Kim, J. Szanyi and C.H.F. Peden, J. Phys. Chem. C 112 (2008) 9486-9492.
26. C. Pecharromn, I. Sobrados, J.E. Iglesias, T. Gonzlez-Carreo and J. Sanz, J. Phys. Chem. B 103 [30], (1999) 6160-6170.
27. X.Y. Chen, Z.J. Zhang, X.L. Li and S.W. Lee, Solid State Commun. 145 (2008) 368-373.
28. D. Kuang, Y. Fang, H. Liu, C. Frommen and D. Fenske, J. Mater. Chem. 13 (2003) 660-662.
29. X. Zhang, Z. Wen, Z. Gu, X. Xu and Z. Lin, J. Solid State Chem. 177 (2004) 849-855.